Chemistry–A European Journal
Research Article
doi.org/10.1002/chem.202203399
Chemistry Europe
European Chemical Societies Publishing
www.chemeurj.org

Experimental and Theoretical Exploration of ESIPT in a Systematically Constructed Series of Benzimidazole Based Schiff Base Probes: Application as Chemosensors

Riya Bag,*[a] Yeasin Sikdar,[a, b] Sutapa Sahu,[a] Md Majharul Islam,[c] Sukhendu Mandal,[c] and Sanchita Goswami*[a]

Abstract: Herein, we have utilized 2-(2-hydroxyphenyl)benzimidazole (HBI) to synthesize 3-(1H-benzoimidazol-2-yl)-2-hydroxy-5-methyl-benzaldehyde (HBIA) followed by three Schiff bases by using *–ortho* (**H_2BIo**), *-meta* (**H_3BIdm**) and *-para* (**H_2BIp**) substituted amino benzoic acids and studied their photophysical properties. We have successfully derived molecular structures of HBI, HBIA and **H_3BIdm** which reveals that in HBI and HBIA, the phenolic –OH is intramolecularly hydrogen bonded with sp^2 N of benzimidazole group whereas in **H_3BIdm**, it is hydrogen bonded with imine C=N of Schiff base moiety, which is responsible for different solid state emission properties of the reported compounds. Extensive experimental and theoretical studies show that for all three Schiff bases, in solution due to activation of C=N isomerization, ESIPT operates through benzimidazole site and displays different emission from the solid state. Furthermore, **H_2BIo**, **H_3BIdm** and **H_2BIp** selectively sense Cu^{2+} in semi aqueous medium with nano-molar detection limit and in HuH-7 cells through the inhibition of ESIPT of process.

Introduction

During past two decades, luminescent organic materials based on excited state intramolecular proton transfer (ESIPT) gained immense attention because of its broad range of applications in chemical and biological systems.[1,2] At 1955, ESIPT was first reported by Weller in methyl salicylate.[3] In ESIPT process, basically a photo-tautomerization occurs in the excited state *via* intramolecular hydrogen bonded chelate. The fundamental requirement of ESIPT process is the presence of both acidic and basic moieties in close proximity within a molecule. In general, molecules having intramolecular hydrogen bonding interaction between a proton donor (–OH/–NH) and proton acceptor (–C=O/heterocyclic N) are ideal candidates to exhibit ESIPT phenomenon. ESIPT process comprises of the following four levels of photochemical processes: (i) excitation from ground state of the enol from to first excited state (enol→enol*), (ii) charge distribution in the excited state increases acidity and basicity of proton donor and acceptor group which leads to proton transfer from donor to acceptor and converts enol*→keto*, (iii) in the next step with the emission of fluorescence, keto* returns to the keto form (keto*→keto) and (iv) in final step, due to thermodynamical instability of keto form, it comes back to the more stable enol form (keto→enol) (Scheme S1).[4] Due to this rapid four-level photochemical process, ESIPT active molecules generally exhibit dual emission: (i) enol emission at shorter wavelength and (ii) keto emission at higher wavelength. As photo-tautomerization is the key requirement for ESIPT process, so blocking of donor-H···acceptor interaction leads to loss of keto emission with the inhibition of ESIPT process. In this context polar or H-bonding solvents can suppress ESIPT process by forming intermolecular hydrogen bond.[4]

ESIPT operative organic compounds, owing to their multiple photophysical properties, such as, dual fluorescence, large Stokes' shifts and photostability, find suitable analytical applications as fluorescence chemosensors. Till now several groups have reported ESIPT based fluorophores for selective sensing of environmentally and biologically important analytes.[5–8] The sensing of analyte by ESIPT active sensor is based on either destroying the donor-H···acceptor bond by the analyte or regeneration of donor-H···acceptor bond through breaking of donor-blocking agent bond. The system significantly contributed to ESIPT research is 2-(2-hydroxyphenyl)benzothiazole (HBT),[9–13] in which phenolic –OH acts as proton donor, while nitrogen of thiazole ring serves as proton acceptor.[14]

Based on the above discussion, herein we have taken 2-(2-hydroxyphenyl)benzimidazole (HBI) in place of 2-(2-hydroxyphenyl)benzothiazole (HBT) and then incorporated an aldehyde group at the sixth position of HBI compound to

[a] *Dr. R. Bag, Dr. Y. Sikdar, Dr. S. Sahu, Dr. S. Goswami*
Department of Chemistry
University of Calcutta
92, A.P.C. Road, Kolkata-700009 (India)
E-mail: riyabag.chem@gmail.com
sgchem@caluniv.ac.in
[b] *Dr. Y. Sikdar*
Department of Chemistry
The Bhawanipur Education Society College
5, Lala Lajpat Rai Sarani, Kolkata-700020 (India)
[c] *M. Majharul Islam, Dr. S. Mandal*
Department of Microbiology
University of Calcutta
35, Ballygunge Circular Road, Kolkata-700019 (India)
Supporting information for this article is available on the WWW under https://doi.org/10.1002/chem.202203399

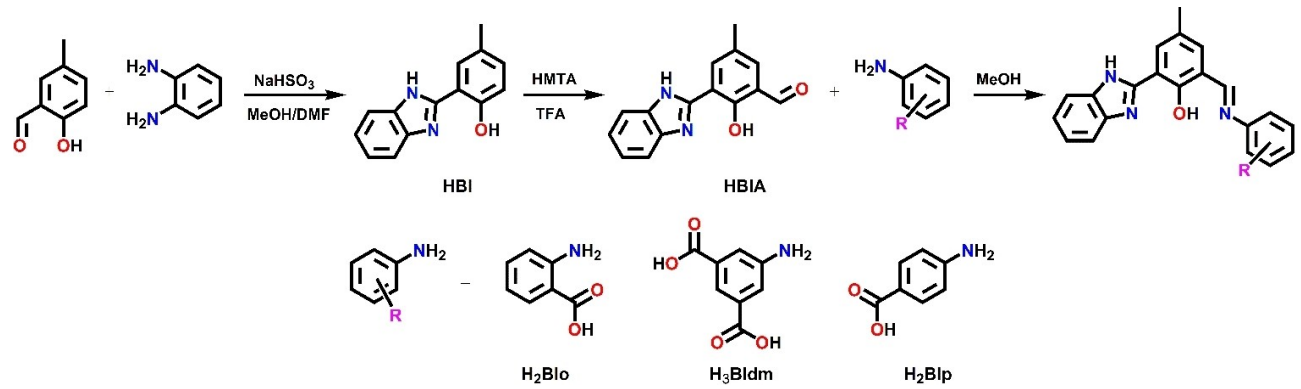

Scheme 1. Synthetic scheme of **H_2BIo**, **H_3BIdm** and **H_2BIp**.

generate HBIA (3-(1H-benzoimidazol-2-yl)-2-hydroxy-5-methyl-benzaldehyde) and finally synthesized three Schiff bases, 2-{[3-(1H-benzoimidazol-2-yl)-2-hydroxy-5-methyl-benzylidene]-amino}-benzoic acid (**H_2BIo**), 5-{[3-(1H-benzoimidazol-2-yl)-2-hydroxy-5-methyl-benzylidene]-amino}-isophthalic acid (**H_3BIdm**) and 4-{[3-(1H-benzoimidazol-2-yl)-2-hydroxy-5-methyl-benzylidene]-amino}-benzoic acid (**H_2BIp**) by using HBIA and *-ortho*, *-meta* and *-para* substituted amino benzoic acids and studied their ESIPT properties. We have successfully derived molecular structures of HBI, HBIA and **H_3BIdm**. Furthermore, to support the experimental results, extensive DFT/TD-DFT calculations have been performed. In addition, we have employed these ESIPT exhibiting compounds as sensing platform and all the three probes successfully sense Cu^{2+} with nano-molar detection limits in semi aqueous medium and in complex matrix of live cells.

Results and Discussion

Design, syntheses and general characterization

Excellent fluorescence property of 2-(2-hydroxyphenyl)benzimidazole (HBI) group prompted us to design and synthesize three structurally similar benzimizaole-amino benzoic acid analogues, **H_2BIo**, **H_3BIdm** and **H_2BIp**, which is depicted in Scheme 1. In ^{1}H NMR spectra of the probes (Figures S5, S7 and S9), H_c (imine proton) appears at slightly downfielded region compared to HBIA (Figure S3) indicating formation of Schiff base. In ESI-MS spectra, presence of molecular ion peak at 372.1515 amu [(**H_2BIo** + H)$^+$], 416.1856 amu [(**H_3BIdm** + H)$^+$] and 372.1476 amu [(**H_2BIp** + H)$^+$] confirms the formation of respective probes (Figures S13–S15). Furthermore, in FT-IR spectra of Schiff base compounds shows $\nu_{(C=N)}$ at 1620 cm^{-1} (**H_2BIo**), 1625 cm^{-1} (**H_3BIdm**) and 1600 cm^{-1} (**H_2BIp**). The peak for –C=O group appears at 1675 cm^{-1} for both **H_2BIo** and **H_2BIp**, while FT-IR spectra of **H_3BIdm** shows two peaks at 1726 cm^{-1} and 1676 cm^{-1} corresponding to two –C=O groups (Figures S20–S22). The ^{1}H, ^{13}C NMR, ESI-MS and FT-IR spectra are given in the Figures S1–S22.

SC-XRD study

The single crystal structure determination was carried out for the probe **H_3BIdm** and its precursor HBI and HBIA to elucidate the hydrogen bonding behaviour of phenolic –OH (donor) to the two potential hydrogen bonding acceptor sites (sp^2 N of benzimidazole vs. –CHO and –CH=N) in solid state to establish the ESIPT mechanism. HBI, HBIA and **H_3BIdm** were crystallized in monoclinic *P21/c*, tetragonal *I-4*, orthorhombic *Pbcn* space group respectively (Figure 1). The most common features of these three ligands are the presence of benzimidazole group *-ortho* to the phenolic group. In all the molecules the C–O, C–N and C=N bond lengths are in the acceptable range to the similar compounds in literature.[15–17] In solid state the dihedral angle between the phenolic group and benzimidazole group decreases with increase in the functionalization of the *-ortho*

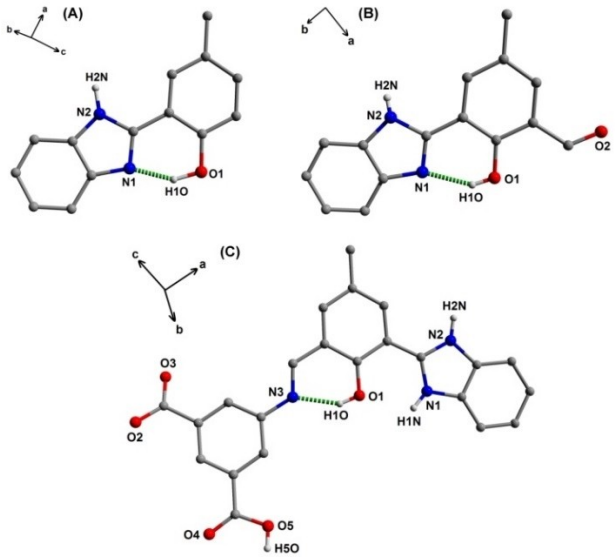

Figure 1. Molecular structures of A) HBI, B) HBIA and C) **H_3BIdm**. Hydrogen atoms attached to carbon and two solvent molecules in **H_3BIdm** were not shown for clarity. Color code: C = grey; N = blue; O = red; H = light grey, Hydrogen bond = green.

group, 5.08° in HBI, 3.75° in HBIA and 2.24° in **H_3BIdm**. Thus, we can assume that derivatisation of HBI leads to a more planar molecule. In HBI and HBIA, the phenolic –OH is intramolecularly hydrogen bonded with sp^2 N of benzimidazole group whereas in **H_3BIdm** it is hydrogen bonded with imine C=N of Schiff base moiety (Table S1). Another interesting feature of **H_3BIdm** is the simultaneous presence of acidic $-CO_2H$ of 5-amino-isophthalic acid and basic N of benimidazole leads protonation of sp^2 N (N1) of benzimidazole and deprotonation of $-CO_2H$ group. Crystallographic data and the metric parameters of all three structures are tabulated in Tables S2 and S3, respectively. The phase purity of all three compounds were confirmed by the powder XRD experiment which shows comparable peak position of experimental and simulated SC-XRD patterns (Figure S23).

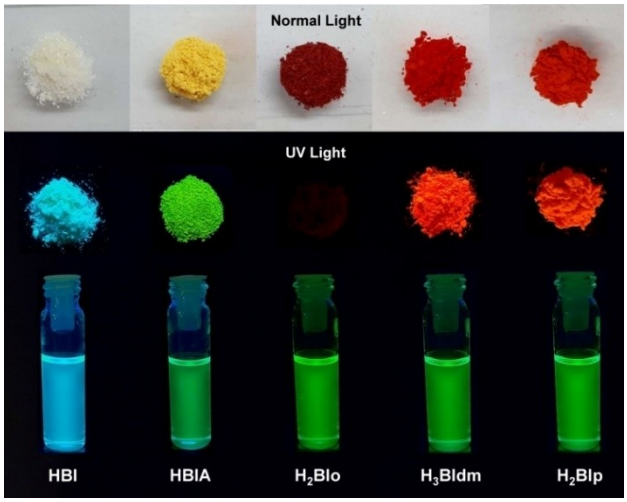

Figure 2. Visualization of fluorescent compounds, HBI, HBIA, **H_2BIo**, **H_3BIdm** and **H_2BIp** in solid and DMSO medium under UV light.

Photophysical studies

Existence of ESIPT liable intramolecular O–H···N hydrogen bond within the system allows us to check emission properties of all three probes in various solvents as well as in solid state. So, we initiated our experiment by recording solid state absorption and emission spectra of the synthesized compounds. Under UV lamp, solid compounds of HBI and HBIA show sky blue and green fluorescence respectively which indicates solid state ESIPT phenomenon (Figure 2).[18,19] Upon excitation at 358 nm, solid HBI shows strong emission at 470 nm, whereas on excitation at 380 nm, solid HBIA shows strong emission at 520 nm (Figure 3A). As in solid state, in solution, HBI and HBIA also show sky blue and green fluorescence respectively through ESIPT mechanism (Figure 2). Upon excitation at 350 nm, HBI shows a strong emission at 470 nm (Figure 3B), whereas upon excitation at 360 nm HBIA shows dual emission at 510 nm and 430 nm (Figure 3B). **H_3BIdm** and **H_2BIp** show slight orange fluorescence (Figure 2) with emission maxima at 610 nm and 620 nm respectively in the solid state (Figure 3A) but on the contrary, **H_2BIo** does not show any fluorescence (Figures 2 and 3A). It can be observed from Figure 1that in HBI or HBIA, ESIPT active six membered H-bonded chelate ring formation takes place through O–H···N (benzimidazole), but in case of **H_3BIdm** it forms through imine nitrogen which is responsible for weak emission at 610 nm. The *-ortho* analogue (**H_2BIo**) is stabilized further by the H-bonding between $O_{carboxyl}$–H···$O_{phenolic}$, as shown in Scheme 2. So, like **H_3BIdm** or **H_2BIp**, no intramolecular protonation-deprotonaion between sp^2 N of benzimidazole and $-CO_2H$ group is possible for **H_2BIo**. The non-emissive behavior of **H_2BIo** in solid state (Figures 2 and 3A) suggests that $O_{carboxyl}$–H···$O_{phenolic}$ bonding interferes with the ESIPT phenomenon in someway (Scheme 2).

Surprisingly, in DMSO medium all three compounds (**H_2BIo**, **H_3BIdm** and **H_2BIp**) show a green fluorescence (Figure 2) with strong emission at 512 nm and a weak emission at 410 nm (Figure 3B), i.e., completely different emission spectra were generated in solid and solution. In polar solvents, compounds of HBI can exist as *cis*-enol (I) and open-enol (I′) conformers (Scheme S2).[20] The existence of this conformational equilibrium

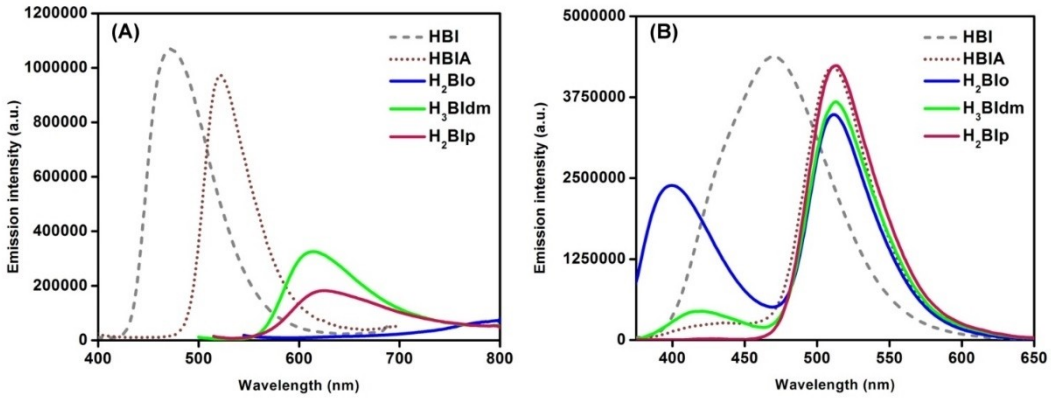

Figure 3. Emission spectra of HBI, HBIA, **H_2BIo**, **H_3BIdm** and **H_2BIp** in A) solid and B) DMSO medium.

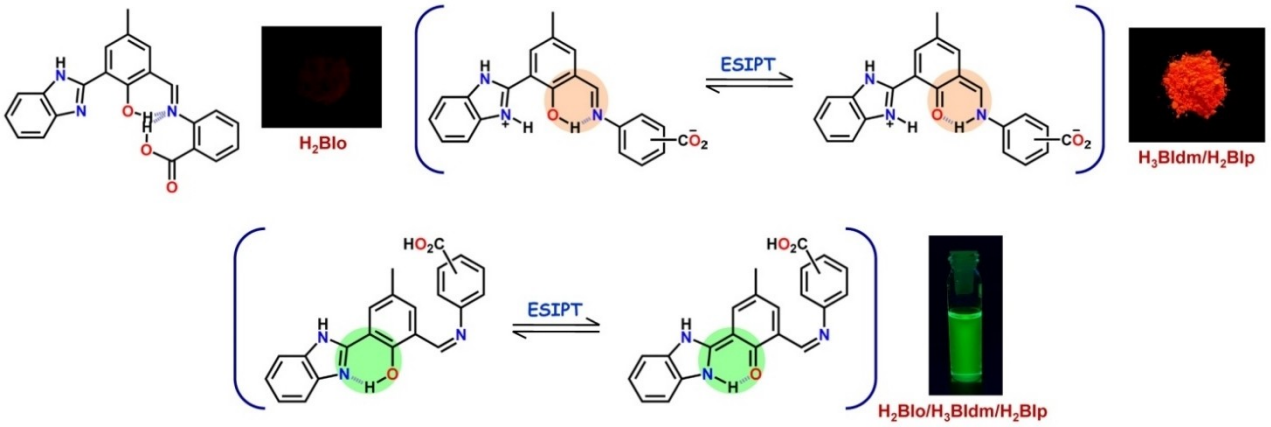

Scheme 2. Schematic representation of structure dependent emission behavior of **H_2BIo**, **H_3BIdm** and **H_2BIp** in solid and solution state.

in the solution is responsible for dual emission, with longer wavelength emission at 512 nm corresponding to excited keto emission and a weak blue-shifted emission at 410 nm due to the open-enol conformer ascribed to normal emission. The existence of this conformational equilibrium is further confirmed by the different position and nature of the peak in the excitation spectra of synthesized compounds at the two emission wave lengths (Figure S24). With the excited keto emission wavelength, the obtained excitation spectra (Figure S24B) completely resemble with the absorption spectra (Figure 4A), while with the normal emission wavelength, the nature and/or position of the peak (Figure S24C) did not remain the same. This implies that a major amount of *cis*-enol (I) exist in the ground state.

The absorption spectra also give different outputs. In solid state all three compounds are red in color (Figure 2) with absorption maxima at 500 nm, 484 nm and 498 nm for **H_2BIo**, **H_3BIdm** and **H_2BIp** respectively (Figure S25A). Whereas, in DMSO medium **H_2BIo** show absorption maxima at 340 nm and 306 nm, **H_3BIdm** show bands at 360 nm and 275 nm and **H_2BIp** has absorption maxima at 367 nm, 340 nm and 295 nm (Figure S25B). This different outcome of solid and solution phase is the results of combined effect of two well-known florescence mechanisms, ESIPT and C=N isomerization. Molecular structure of HBIA reveals, in solid state, the –C=O bond is at *trans* position and phenolic proton forms H bond with benzimidazole nitrogen, on the other hand, in the solid state structure of **H_3BIdm**, imine bond (–C=N) is at *cis* position and phenolic proton forms H bond with imine nitrogen. But in solution medium, due to facile C=N isomerization, imine bond is at *trans* position and phenolic hydrogen rotates towards benzimidazole ring and forms ESIPT active six membered H-bonded chelate ring with benzimidazole nitrogen. So, in solid state, due to inhibition of C=N isomerization, only ESIPT is operative through imine site and hence weak emission was observed, on the other hand, in DMSO, due to activation of C=N isomerization, ESIPT operates through benzimidazole site and emits strongly like HBIA (Scheme 2).

We have then proceeded to study ESIPT phenomenon of the synthesized compounds in different organic media and aqueous solution. In organic solvents, like CH_3CN, EtOH, MeOH, IPrOH, DMSO and DMF, **H_2BIo** shows peaks at 340–327 nm and 295–306 nm, in addition a new peak at 420 nm and 448 nm was observed in IPrOH and DMF medium respectively (Figure 4A, Table S4). In aqueous medium, **H_2BIo** generates completely new spectra with absorption maxima at 420 nm and 303 nm (Figure 4A). We then further recorded absorption spectra of **H_2BIo** in semi aqueous medium and it showed that

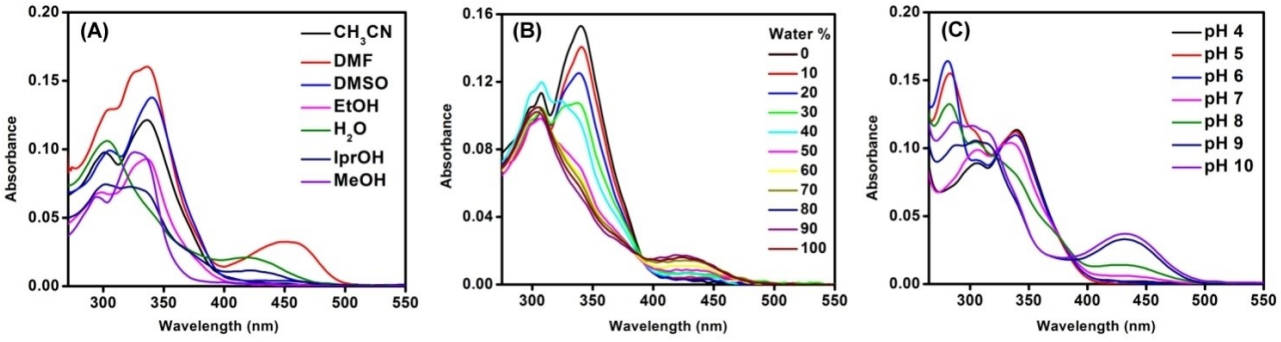

Figure 4. UV-Vis absorption spectra of **H_2BIo** in A) different solvents, B) semi aqueous medium and C) at different pH.

with increasing amount of water, the absorbance at 340 nm continues to decrease and the peak at 420 nm gradually increased (Figure 4B). Generation of red shifted peak in aqueous medium indicates formation of anionic species of the probe. This was further confirmed by taking absorption spectra of **H_2BIo** with the variation of pH (Figure 4C). Presence of strongly electron withdrawing $-CO_2H$ group in the system makes –OH proton sufficiently acidic and facilitates formation of **HBIo$^-$** in aqueous medium. In this context *-meta* (**H_3BIdm**) and *-para* (**H_2BIp**) substituted probes show similar behavior as like *-ortho* substituted probe (**H_2BIo**) in organic and aqueous medium (Figures S26 and S27, Table S4).

Upon excitation at 340–330 nm, **H_2BIo** shows dual emission at 500–512 nm (keto emission) and 400–407 nm (normal emission) in CH_3CN, DMSO and DMF (Figure 5A). In alcoholic medium (EtOH, MeOH and IPrOH) 30–40 nm blue shift in keto emission (470 nm), whereas, in normal emission, 4–5 nm blue shift was observed (Figure 5A). The possibility of extensive H-bonding in polar protic solvents becomes responsible for the blue-shifted keto emission compared to polar aprotic solvents. In polar aprotic solvents, along with *cis*-enol (I), normal open-enol (I') is present (Scheme S2). However, H-bonded conformers are present in polar protic solvents (Scheme S2). In polar aprotic solvents, both the open-enol and keto forms showed a mono-exponential decay pattern with lifetime values of 6.96–8.76 ns and 4.28–4.53 ns respectively (Figure S30, Table 1). But in polar protic solvents (EtOH and MeOH), a bi-exponential decay pattern was observed in both emission wavelengths (Figure S30, Table 1). In the case of a more hindered alcohol, IPrOH, only one H-bonded species was observed in the excited state (Figure S30, Table 1). Like **H_2BIo**, **H_3BIdm** also shows dual emission at 504–525 nm and 405–415 nm in all the studied solvents except MeOH where keto emission appeared at 473 nm (Figure S28A). *-Para* substituted ligand, **H_2BIp**, on the other hand, shows only keto emission at 505–525 nm in CH_3CN, IPrOH, DMSO and DMF medium and 480 nm in EtOH and MeOH medium (Figure S29A). In **H_2BIp**, due to –R effect of $-CO_2H$ group at *-para* position with consequent extended conjugation, phenolic hydrogen becomes more acidic and easily undergoes enolisation at excited state and generates only keto emission. We have then measured excited state life time of **H_3BIdm** and **H_2BIp** in different solvents. Like *-ortho* analogue (**H_2BIo**), in polar aprotic solvents both the open-enol and keto forms of **H_3BIdm** showed a mono-exponential decay pattern with lifetime values of 3.25–5.54 ns and 4.23–4.42 ns respectively (Figure S30, Table 1). In case of polar protic solvents, in MeOH medium, keto form showed bi-exponential decay pattern with two differently populated species having lifetime values of 1.66 (26 %) and 4.16 (74 %) ns, but in other two protic solvents, it showed existence of one species in the excited state (Figure S30, Table 1). The presence of two carboxylic groups at the *-meta* position, as well as hydrogen bonding with more alkyl group substituted alcohol, might be responsible for the existence of single species in the excited state for **H_3BIdm** in EtOH and IPrOH medium. Again, in case of keto form of *-para* analogue (**H_2BIp**) a bi-exponential decay pattern was observed in EtOH and MeOH

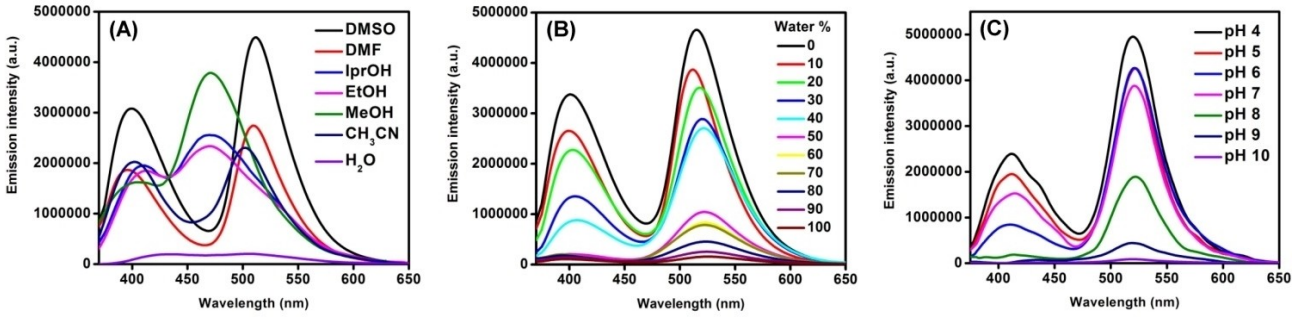

Figure 5. Emission spectra of **H_2BIo** in A) different solvents, B) semi aqueous medium and C) at different pH.

Table 1. Excited state lifetime parameters of **H_2BIo**, **H_3BIdm** and **H_2BIp** in different solvents.

Solvent	**H_2BIo**				**H_3BIdm**				**H_2BIp**			
	λ_{em} [nm]	τ_1 [ns]	τ_2 [ns]	τ_{av} [ns]	λ_{em} [nm]	τ_1 [ns]	τ_2 [ns]	τ_{av} [ns]	λ_{em} [nm]	τ_1 [ns]	τ_2 [ns]	τ_{av} [ns]
DMSO	512	4.53	–	–	512	4.42	–	–	512	4.46	–	–
	404	8.76	–	–	420	5.54	–	–				
DMF	510	4.41	–	–	510	4.33	–	–	510	4.34	–	–
	400	7.91	–	–	410	4.73	–	–				
IPrOH	470	4.80	–	–	525	4.80	–	–	525	4.79	–	–
	410	8.08	–	–	420	5.34	–	–				
EtOH	470	4.64(82 %)	7.96(18 %)	5.23	525	4.74	–	–	480	0.03(62 %)	4.46(38 %)	1.71
	410	1.18(15 %)	8.24(85 %)	7.18	422	1.44(43 %)	5.53(57 %)	3.78				
MeOH	470	1.07(23 %)	4.21(77 %)	3.49	473	1.66(26 %)	4.16(74 %)	3.51	475	2.51(31 %)	4.43(69 %)	3.83
	402	2.25(59 %)	4.92(41 %)	3.34	402	2.00(41 %)	3.60(59 %)	2.94				
CH_3CN	500	4.28	–	–	504	4.23	–	–	505	4.27	–	–
	400	6.96	–	–	407	3.25	–	–				

medium as like -*ortho* analogue (**H_2BIo**) with lifetime values of 0.03 (62%) and 4.46 (38%) ns for EtOH and 2.51 (31%) and 4.43 (69%) ns for MeOH (Figure S30, Table 1). We have calculated quantum yields of **H_2BIo**, **H_3BIdm** and **H_2BIp** in different solvents which are enlisted in Table 2. Due to insolubility of the synthesized compounds in less polar to non-polar solvents like, $CHCl_3$ and hexane, we are unable to study ESIPT properties of the compounds in these solvents.

We further examined this double emission phenomenon in aqueous medium. However, in 100% aqueous solution, all three probes become non-emissive (Figures 5A, S28 A and S29 A). To get better insight we recorded emission spectra of probes in semi aqueous medium and the emission intensities for both the tautomers gradually decreased with increment of water (Figures 5B, S28B and S29B). The newly generated peak (417–422 nm) in the absorption spectra of all three probes in aqueous medium (Figures 4A, S26A and S27A) indicates generation of anions of the probes, which restricts keto⇌enol tautomerism and became responsible for decreased emission intensity. Hence, emission property of the probe was dependent on basicity of the medium. This was further confirmed by emission intensity vs. pH plot, where increasing pH leads to decrease in emission intensity (Figures 5C, S28C and S29C).

Theoretical calculations and TD-DFT studies

To validate experimental findings, herein we have optimized multiple conformers for each compounds based on C=N isomerization and/or keto-enol tautomerisaion and compared their TD-DFT computed absorption spectra with the experimental ones. In case of starting compound, HBI, enol form (I) is the principle component in the solution, whereas keto form (II) has no stability in ground state. The computed spectral pattern for conformer I (310 nm and 280 nm) matches well with the experimental spectra (330 nm and 292 nm) of HBI but slightly blue shifted (Figure S31). Experimental 330 nm band is correlated with the $S_0 \rightarrow S_1$ (3.994 eV, 310 nm, $f = 0.5032$) electronic transition and 292 nm band is correlated with $S_0 \rightarrow S_2$ (4.460 eV, 278 nm, $f = 0.1801$) and $S_0 \rightarrow S_3$ (4.419 eV, 280 nm, $f = 0.2219$) electronic transitions (Figure S31, Table S5).

For the next compound, HBIA, which shows dual emission phenomena corresponding to open-enol (I′) and excited keto emission, the comparison of the relative energies of the three conformers shows the enol form (I) to be 29.90 kJ/mol and 63.06 kJ/mol more stable than the keto form (II) and open-enol (I′) conformers respectively. HBIA shows two absorption maxima in the experimental spectra at 362 nm and 291 nm. In the calculated TD-DFT spectra of conformer I of HBIA, 362 nm peak corresponds to one single vertical transition ($S_0 \rightarrow S_1$, 3.246 eV, $f = 0.2647$) at 382 nm whereas 291 nm peak corresponds to another single vertical transition ($S_0 \rightarrow S_5$, 4.449 eV, $f = 0.4943$) at 279 nm (Figure S32, Table S6). TD-DFT computed absorption spectra of open-enol conformer (I′) show blue shifted spectra with absorption maxima at 327 nm ($S_0 \rightarrow S_4$, 3.789 eV, $f = 0.1300$) and 246 nm ($S_0 \rightarrow S_5$, 5.040 eV, $f = 0.1377$) (Figure S32, Table S6). A red shifted TD-DFT computed absorption spectra was obtained for keto conformer (II) with absorption maxima at 407 nm ($S_0 \rightarrow S_1$, 3.045 eV, $f = 0.4819$) and 295 nm ($S_0 \rightarrow S_6$, 4.197 eV, $f = 0.2663$) (Figure S32, Table S6). The relative energy, TD-DFT computed spectral pattern and excitation spectra obtained from the open-enol emission wavelength support the co-existence of enol (I) (major) and open-enol (I′) (minor) forms in the solution.

Like HBIA, **H_2BIo** also shows dual emission properties and from the structure optimization and TD-DFT study, it was clear that a minor amount of the open-enol conformer (I′) of HBIA was present in the solution, which becomes responsible for blue-shifted emission. Because Schiff base compounds also exhibit blue-shifted normal emission like HBIA, it could be said that a minor amount of the respective open-enol conformer is present in the solution. As the experimental results indicate that in the synthesized Schiff base compounds (**H_2BIo**, **H_3BIdm** and **H_2BIp**) C=N isomerization modulates the keto-enol tautomerisation site, therefore, in order to identify the major species in solution, here we have optimized total four conformers. Conformers I and III are enol tautomers of *trans* and *cis* isomers respectively, whereas conformers II and IV are keto tautomers of *trans* and *cis* isomers respectively. For all three compounds, comparison of relative energies of four conformers indicates stabilities of enol tautomers over keto tautomers (Figures 6, S33 and S34). The overlay of UV-Vis spectra of Schiff base compounds (**H_2BIo**, **H_3BIdm** and **H_2BIp**) and TD-DFT of conformer I, II, III and IV of the respective compounds shows matching of spectral output in terms position and intensity majorly with the conformer I which concludes existence of *trans*-enol conformer (I) in solution (Figures 6, S33 and S34).

Experimental absorption spectra of **H_2BIo** show two bands at 340 nm and 306 nm. In conformer I, 340 nm and 306 nm bands are correlated with $S_0 \rightarrow S_1$ (3.078 eV, 403 nm, $f = 0.2284$) and $S_0 \rightarrow S_4$ (3.544 eV, 350 nm, $f = 0.1358$) vertical transitions respectively (Figure 6 and Table S7). In conformer II, the low energy band becomes red shifted and appears at 434 nm ($S_0 \rightarrow S_1$, 2.854 eV, $f = 0.5117$), whereas experimental maxima at 306 nm is attributed to multiple vertical transitions, $S_0 \rightarrow S_6$ (4.110 eV, 301 nm, $f = 0.1727$) and $S_0 \rightarrow S_7$ (4.166 eV, 297 nm, $f = 0.1235$) (Figure 6 and Table S8). In conformer III along with absorption bands at 330 nm ($S_0 \rightarrow S_2$, 3.725 eV, $f = 0.6179$, $\lambda = 333$ nm and $S_0 \rightarrow S_5$, 3.973 eV, $f = 0.1135$, $\lambda = 312$ nm) and 286 nm ($S_0 \rightarrow S_6$, 4.255 eV, $f = 0.1812$, $\lambda = 291$ nm; $S_0 \rightarrow S_8$, 4.337 eV, $f = 0.4683$, $\lambda = 289$ nm and $S_0 \rightarrow S_9$, 4.546 eV, $f = 0.1193$, $\lambda = 273$ nm), a new band at 416 nm ($S_0 \rightarrow S_1$, 2.982 eV, $f = 0.2221$) was generated which was absent in experimental spectra (Figure 6 and Table S9). Like conformer III, similar spectral

Table 2. Quantum yields of **H_2BIo**, **H_3BIdm** and **H_2BIp** in different solvents.

Solvent	ϕ (**H_2BIo**)	ϕ (**H_3BIdm**)	ϕ (**H_2BIp**)
DMSO	0.84	0.78	0.80
DMF	0.63	0.67	0.58
IPrOH	0.68	0.62	0.65
EtOH	0.67	0.59	0.62
MeOH	0.70	0.68	0.75
CH_3CN	0.67	0.60	0.69
H_2O	0.05	0.04	0.05

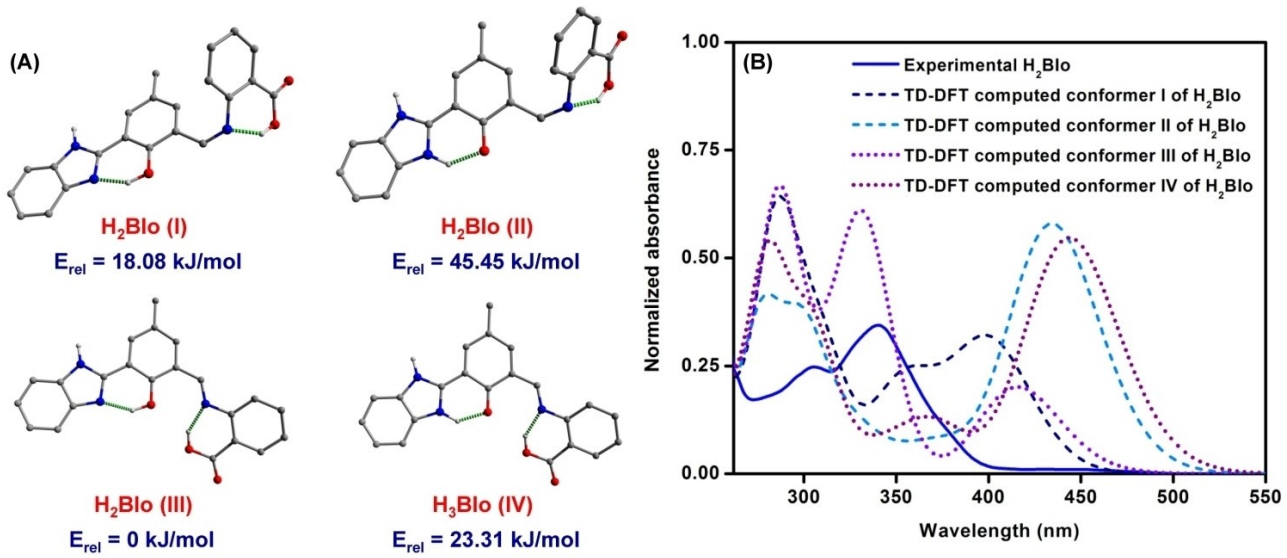

Figure 6. A) DFT-B3LYP optimized molecular structures of **H_2BIo** and B) Correlation between experimental and TD-DFT computed UV-Vis absorption spectra of **H_2BIo**.

pattern was observed for conformer IV but with red shifted absorption bands. Low energy band at 444 nm is attributed to one single vertical transition, $S_0 \rightarrow S_1$ (2.793 eV, $f = 0.6044$), while other two bands at 370 nm ($S_0 \rightarrow S_3$, 3.345 eV, $f = 0.0985$) and 280 nm ($S_0 \rightarrow S_5$, 4.019 eV, $f = 0.2042$, $\lambda = 308$ nm; $S_0 \rightarrow S_6$, 4.107 eV, $f = 0.1708$, $\lambda = 302$ nm; $S_0 \rightarrow S_8$, 4.325 eV, $f = 0.1031$, $\lambda = 286$ nm and $S_0 \rightarrow S_{10}$, 4.437 eV, $f = 0.4097$, $\lambda = 279$ nm) are attributed to multiple vertical transitions (Figure 6 and Table S10). For other two ligands (**H_3BIdm** and **H_2BIp**) similar type of spectral patterns are observed (Figures S33 and S34). Details of the TD-DFT results are tabulated in Tables S11–S18. So, the TD-DFT outcome also suggests that in solution imine bond becomes *trans* and keto-enol tautomerisation occurs through benzimidazole site.

Based on the photophysical properties of **H_2BIo** and the molecular structure of **H_3BIdm** in the solid state, we have also optimized the molecular structure of **H_2BIo** (conformer V) that can exist in the solid state (Figure 7). The solid state absorption spectra of **H_2BIo** show three bands at 512 nm, 386 nm and 333 nm. The TD-DFT computed absorption spectra of conformer V also show three peaks both in gas (434 nm, 335 nm and 284 nm) as well as solution medium (449 nm, 337 nm and 285 nm) but with slightly blue shifted absorption maxima (Figure 7 and Table S19). The TD-DFT computed spectral pattern and non-emissive nature of **H_2BIo** both support existence of the conformer V in the solid state.

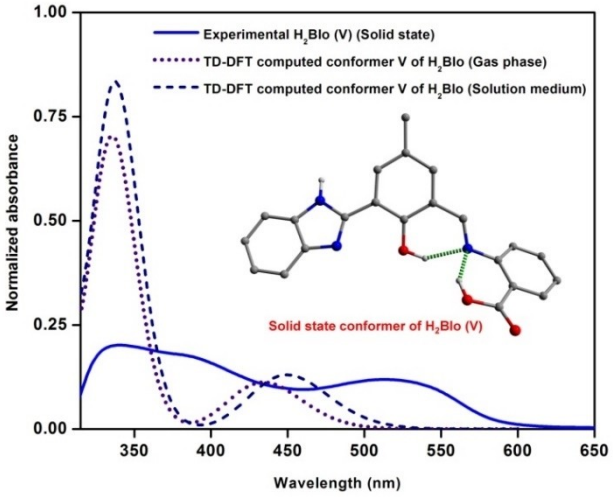

Figure 7. DFT-B3LYP optimized molecular structure and correlation between experimental and TD-DFT computed UV-Vis absorption spectra of solid state conformer of **H_2BIo**.

Analytical studies

We investigated the sensing capabilities of these fluorescent probes in presence of various metal ions such as, Na^+, K^+, Ca^{2+}, Mg^{2+}, Al^{3+}, Cr^{3+}, Fe^{3+}, Fe^{2+}, Mn^{2+}, Co^{2+}, Ni^{2+}, Cu^{2+}, Zn^{2+}, Cd^{2+} and Hg^{2+} in (7:3) DMSO:HEPES-buffer solution (25 mM, pH = 7.2). A significant quenching in emission spectra ($\lambda_{ex} = 340$ nm, $\lambda_{em} = 512$ nm, **H_2BIo**; $\lambda_{ex} = 360$ nm, $\lambda_{em} = 512$ nm, **H_3BIdm**; $\lambda_{ex} = 360$ nm, $\lambda_{em} = 512$ nm, **H_2BIp**) of **H_2BIo**, **H_3BIdm** and **H_2BIp** with change in color of the solution from green to color less under UV lamp was observed in presence of Cu^{2+} ion, whereas no significant spectral changes were observed for other metal ions (Figure 8, Figure 9 and Table S20). The competitive experiment was performed to validate the selectivity of these probes towards Cu^{2+} (Figure S35). To assure applicability these probes for sensing of Cu^{2+} in waste water effluent, emission spectra of **H_2BIo**, **H_3BIdm** and **H_2BIp** were recorded with different salts (Cl^-, Br^-, NO_3^-, ClO_4^-, OAc^- and SO_4^{2-}) of Cu^{2+} and anion independent sensing of Cu^{2+} was observed (Figure S36).

Figure 8. Visual color change of **H_2Blo** under UV light ($\lambda = 254$ nm) with addition of different metal ions in (7:3) DMSO:HEPES-buffer solution (25 mM, pH = 7.2).

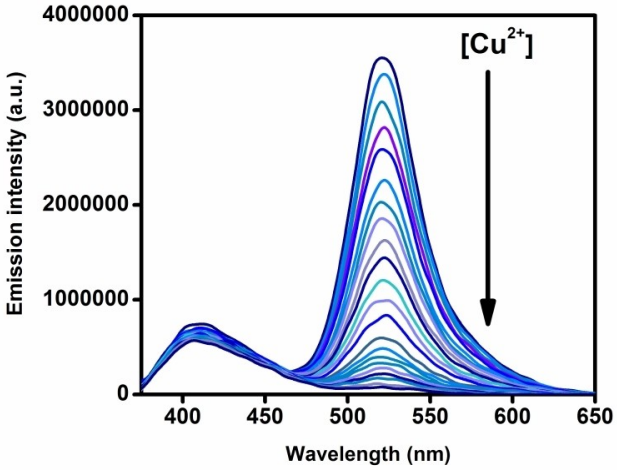

Figure 10. Emission titration spectra of **H_2Blo** (0.1 μM) upon incremental addition of Cu^{2+} in (7:3) DMSO:HEPES-buffer solution (25 mM, pH = 7.2).

Furthermore, Cu^{2+} quenched the emission intensity of **H_2Blo**, **H_3Bldm** and **H_2Blp** at the pH range 4–10 (Figure S37).

To get better insight, we have carried out emission titration experiment by adding increasing concentration of Cu^{2+} to the solution of **H_2Blo**, **H_3Bldm** and **H_2Blp** the emission intensity at 512 nm continuously decreased (Figures 10 and S38). Furthermore, the absorption profile of **H_2Blo**, **H_3Bldm** and **H_2Blp** in presence of Cu^{2+} have shown a new peak around 410–420 nm and each titration profile exhibits an isosbestic point indicating the presence of equilibrium between two species (Figure S39). Moreover, the emission intensity at 512 nm can be reversibly switched by alternative addition of Cu^{2+} and EDTA, permitting **H_2Blo**, **H_3Bldm** and **H_2Blp** to act as a reversible fluorescent sensor for Cu^{2+} (Figure S40).

The calculated limit of detection (LOD = $3\sigma/s$, where, σ is the standard deviation of the blank solution and s is the slope of the calibration curve) of Cu^{2+} by **H_2Blo**, **H_3Bldm** and **H_2Blp** from emission titration experiment were 26.2 nM, 47.2 nM and 45.5 nM respectively (Figure S41), which are much lower than the permissible limit Cu^{2+} in drinking water directed by WHO. To determine binding stoichiometry between probes and Cu^{2+}, Job's plots are constructed and it indicates 1:1 complexation between ligand:Cu^{2+} (Figure S42). Based on 1:1 complexation, Benesi-Hildebrand Equation (1),[21,22]

$$\frac{1}{I_x - I_0} = \frac{1}{I_{max} - I_0} + \left\{ \left(\frac{1}{I_{max} - I_0} \right) \left(\frac{1}{K_a [C]^n} \right) \right\} \quad (1)$$

where, I_0, I_x and I_{max} are the emission intensities of probes in the absence of Cu^{2+}, with intermediate concentration of Cu^{2+} and the concentration of Cu^{2+} at saturation level, respectively, [C] is the concentration of Cu^{2+}, n refers to the number of Cu^{2+} ions associating with each molecule of probes and K_a is the association constant, has been used to determine association constant. A plot of $\{(I_{max}-I_0)/(I_x-I_0)\}$ vs. $1/[Cu^{2+}]^{1/2}$ yields association constant 3.55×10^6 M^{-1} for **H_2Blo**, 2.22×10^6 M^{-1} for **H_3Bldm** and 2.36×10^6 M^{-1} for **H_2Blp**, which indicates Cu^{2+} has more affinity towards **H_2Blo** over **H_3Bldm** and **H_2Blp** (Figure S43). As **H_2Blo** have an extra coordination site in form of *o*-carboxylate group which provide an extra stability to **H_2Blo**-Cu^{2+} complex compared to other two Cu^{2+} complexes (carboxylate are far apart to chelation) and hence **H_2Blo** has higher association constant as well as lower limit of detection for Cu^{2+} than **H_3Bldm** and **H_2Blp**. The ESI-MS spectra of all three ligand-metal complexes show peaks for $[(H_nL)Cu+H]^+$ and $[(H_nL)_2Cu_{2+}H]^+$ fragments at 433.0505 $[(HBlo)Cu]^+$, 865.0859 $[(Blo)_2Cu_{2+}H]^+$, 477.0455 $[(H_2Bldm)Cu]^+$, 955.0247 $[(HBldm)_2Cu_{2+}H]^+$ amu, 433.0548 $[(HBlp)Cu]^+$ and 865.0920 $[(Blp)_2Cu_{2+}H]^+$ (Figures S16–S18). On complexation, $\nu_{(C=N)}$ shifts to lower region compared to free ligands, which indicates complexation through imine nitrogen. Furthermore, in all the complexes, $\nu_{(C=O)}$ and $\nu_{(C-O)}$ also shifts to lower region which indicates deprotonation of $-CO_2H$ group, but a noticeable change either

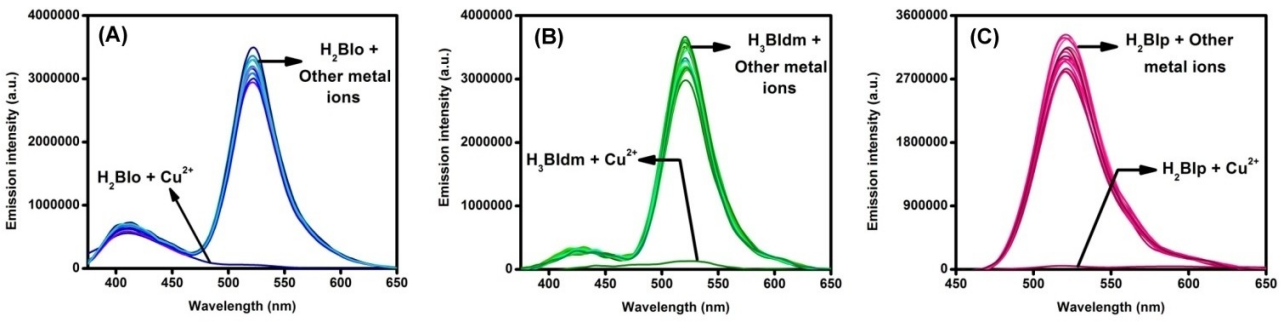

Figure 9. Emission spectra of A) **H_2Blo** (0.1 μM), B) **H_3Bldm** (0.1 μM) and C) **H_2Blp** (0.1 μM) upon addition of 5 equivalents metal ions in (7:3) DMSO:HEPES-buffer solution (25 mM, pH = 7.2).

in peaks position or in shape were observed for *-ortho* analogue compared to *-meta* and *-para* compounds, which supports involvement of carboxylate group in coordination of Cu^{2+} in case of *-ortho* analogue (Figures S20–S22).[23–24] Finally, the fluorescence quenching of the probes in presence of Cu^{2+} is the consequence of inhibition in ESIPT process during complexation with Cu^{2+} (Scheme 3).

Application of H_2Blo, H_3Bldm and H_2Blp for Cu^{2+} detection in live cells

It has been found that the synthesized probes, **H_2Blo**, **H_3Bldm** and **H_2Blp** selectively interact with Cu^{2+} to turn-off their fluorescence. The probes were further investigated for detection of intracellular Cu^{2+} using fluorescence microscopy. Human cancer cell HuH-7 was used as model. Before assessing the intracellular Cu^{2+}, we have performed the cytotoxic effect of the probes and probe-Cu^{2+} complexes on live cells. The MTT assay[25] was adopted to study cytotoxicity of probes and probe-Cu^{2+} complexes at varying concentrations. A cytotoxicity measurement for each experiment shows that the **H_2Blo**, **H_3Bldm** and **H_2Blp** do not have any toxicity on the tested Human cancer cell HuH-7 and $[(Blo)_2Cu_2]$, $[(HBldm)_2Cu_2]$ and $[(Blp)_2Cu_2]$ complexes do not apply significant effect on cell viability at tested concentrations (Figure S44).

Fluorescence microscopic studies revealed bright green fluorescence in HuH-7 cells when treated with the probes (**H_2Blo**/**H_3Bldm**/**H_3Blp**) alone (Figure 11). Upon incubation with (**H_2Blo**/**H_3Bldm**/**H_3Blp**) followed by Cu^{2+}, the existing fluorescence of the probe treated HuH-7 cells have been turned-off. The fluorescence microscopic analysis strongly suggested that probes (**H_2Blo**/**H_3Bldm**/**H_3Blp**) and Cu^{2+} could readily cross the membrane barrier of the HuH-7 cells. It is significant to mention here that bright field images of treated cells did not reveal any gross morphological changes, which suggested that HuH-7 cells were viable.

Conclusion

In this paper, we have systematically designed three benzimizaole-aminobenzoic acid bearing Schiff base probes, 2-{[3-(1H-benzoimidazol-2-yl)-2-hydroxy-5-methyl-benzylidene]-amino}-

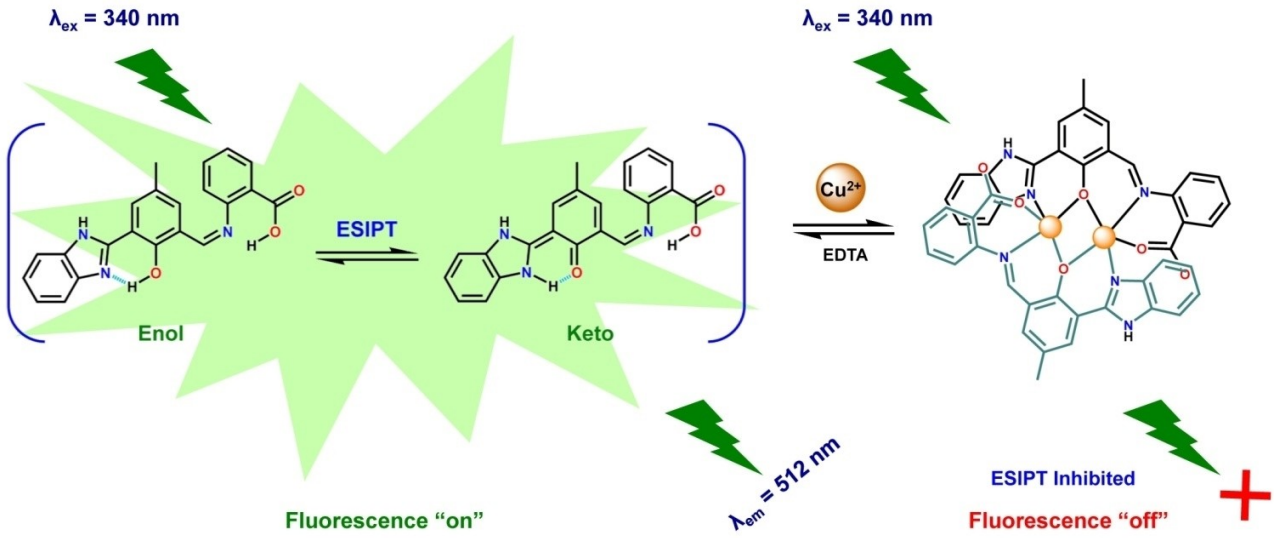

Scheme 3. Proposed sensing mechanism of Cu^{2+} by **H_2Blo**.

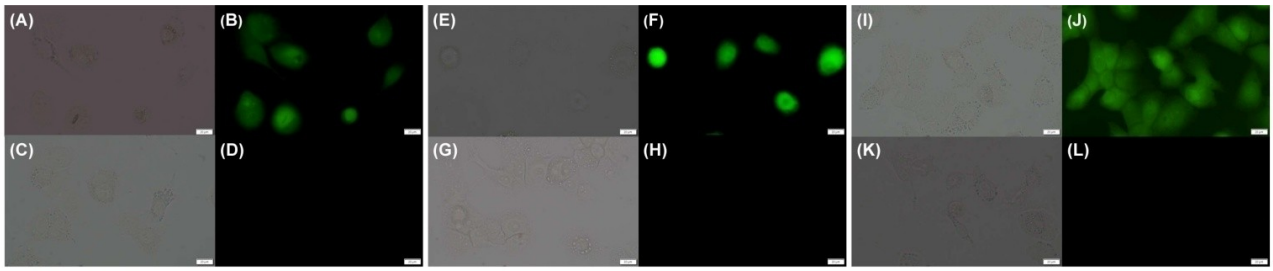

Figure 11. Fluorescence microscopic images of HuH-7 cells: A and B) Cells treated with **H_2Blo** (1 μM); C and D) Cells treated with **H_2Blo** and Cu^{2+} (2.5 μM); E and F) Cells treated with **H_3Bldm** (1 μM); G and H) Cells treated with **H_3Bldm** and Cu^{2+} (2.5 μM); I and J) Cells treated with **H_2Blp** (1 μM); K and L) Cells treated with **H_2Blp** and Cu^{2+} (2.5 μM). All images were acquired with a 40× objective lens.

benzoic acid (**H_2BIo**), 5-{[3-(1H-benzoimidazol-2-yl)-2-hydroxy-5-methyl-benzylidene]-amino}-isophthalic acid (**H_3BIdm**) and 4-{[3-(1H-benzoimidazol-2-yl)-2-hydroxy-5-methyl-benzylidene]-amino}-benzoic acid (**H_2BIp**) by employing *-ortho*, *-meta* and *-para* substituted aminobenzoic acids with elaborate spectral and crystal structural characterizations. The ESIPT activities have been extensively studied by means of experimental and theoretical calculations. At first, the solid state ESIPT phenomenon has been checked and interestingly, **H_3BIdm** and **H_2BIp** exhibited slight orange fluorescence but **H_2BIo** remained non-fluorescent. On the other hand, different emission spectral outcomes were observed for all the three probes in DMSO solvent. In DMSO, they produced a strong emission and a weak emission corresponding to keto and open-enol forms respectively. This difference in solid and solution behaviors have been analyzed in terms of combined effect of two florescence mechanisms, ESIPT and C=N isomerization. In the solution phase, facile C=N isomerization can take place, and therefore, imine bond is at *trans* position and the phenolic -OH rotates towards benzimidazole ring and forms ESIPT active six membered H-bonded chelate ring with benzimidazole nitrogen. ESIPT activities have been studied in other common organic solvents also and the experimental outputs have been explained by means of -R effects of the substituted groups. These experimental findings are reinforced with the help of detailed DFT/TD-DFT calculations. The three probes, **H_2BIo**, **H_3BIdm** and **H_2BIp** can sense Cu^{2+} in semi aqueous medium and in live cells like HuH-7 *via* fluorescence turn-off mechanism with nano-molar detection and are supported by the necessary experimental parameters.

Experimental Section

Materials and apparatus: 2-Hydroxy-5-methylbenzaldehyde, *o*-phenylenediamine, anthranilic acid, 4-aminobenzoic acid, 5-amino-isophthalic acid and HEPES buffer were purchased from Sigma Aldrich. All solvents for synthesis were purchased from commercial sources and used without further purification. Spectroscopic grade organic solvents were used for spectral analysis. Elemental analyses for C, H and N were performed on a Perkin-Elmer 2400 II analyzer. ^{1}H and ^{13}C NMR spectra were recorded in DMSO-d_6 solvent using TMS as standard on a Bruker AV 300 Supercon Digital NMR system. The FT-IR spectra were recorded using KBr pellet in the range of 4000–400 cm^{-1} on Perkin-Elmer Spectrum 100 spectrometer. The ESI-MS analysis was carried out on Waters Xevo G2-S QTOF mass spectrometer. Powder X-ray diffraction (PXRD) patterns were recorded on a Rigaku SmartLab diffractometer using monochromated Cu-K_α radiation of $\lambda = 1.5405$ Å and a Ni-Beta filter. A Systronics digital pH meter (model 335) was used to adjust the pH of the solution. The absorption and emission spectra were recorded on a Hitachi UV-Vis U-3501 spectrophotometer and HORIBA Scientific Fluoromax-4 spectrofluorometer respectively at room temperature in a quartz cuvette with 1 cm path length. Time-resolved fluorescence lifetime measurements were performed with a DeltaFlex Time Correlated Single Photon Counting (TCSPC) spectrometer with a hybrid photomultiplier detector (HPPD). The excitation source was the second harmonic output of a tuneable Mai-Tai Laser ($\lambda_{ex} = 360$ nm) with a pulse picked repetition rate of 8 MHz. The full width at half-maxima (FWHM) of the Instrument Response Function (IRF) was 88 ps.

Evaluation of fluorescence quantum yield: The fluorescence quantum yield was determined using quinine sulphate ($\phi_R = 0.546$ in 0.5 M H_2SO_4) as a reference. The quantum yield is calculated using the Equation (2)

$$\phi_S = \phi_R \times \frac{F_S}{F_R} \times \frac{A_R}{A_S} \times \frac{{\eta_S}^2}{{\eta_R}^2} \quad (2)$$

where, ϕ is the fluorescence quantum yield, *F* terms denotes integrated area under the fluorescence curve, *A* denotes absorbance and η is the refractive index of the medium. Subscripts S and R denote the respective parameters for the studied sample and reference, respectively.[26]

Computational details: All the theoretical calculations reported in this article were done with the ORCA 4.1 program package[27,28] and Avogadro software[29] was used as visualization tool and producing molecular orbital picture. The DFT calculations were performed at the level of Becke three parameter hybrid functional with the non-local correlation functional of Lee-Yang-Parr (B3LYP).[30–33] Gas phase optimized geometry of the ligand and complex were carried out using def2-TZVP,[34–38] a valence triplezeta basis set with new polarization function for all the atom. Resolution of Identity (RI)[39–41] approximation with def2/J auxiliary basis set for Coulomb and HF exchange integral for HF was employed for self-consistent field (SCF) gradient calculations.[42] TD-DFT calculation was performed for the first 75 singlet state with CPCM salvation[43] model using the gas phase optimized coordinate.

Single-crystal X-ray crystallography: X-ray crystallographic data for HBI, HBIA and **H_3BIdm** were collected with Bruker-Nonius APEX-II diffractometers with CCD-area detectors using graphite-monochromated Mo-K_α radiation ($\lambda = 0.71073$ Å) at 296 K. Empirical absorption corrections were applied to the collected reflections using SADABS.[44] The structures were refined on F^2 by full-matrix least-squares technique using the SHELXL16/6 program package.[45] In all cases, non-hydrogen atoms were refined anisotropically. Hydrogen atoms bonded to carbon were refined isotropically in calculated positions. Those bonded to nitrogen and oxygen was located in difference Fourier maps and refined with distance constraints.

Deposition Number(s) 2121175, 2121176 and 2121179contain(s) the supplementary crystallographic data for this paper. These data are provided free of charge by the joint Cambridge Crystallographic Data Centre and Fachinformationszentrum Karlsruhe Access Structures service.

Cell culture: HuH-7 cell lines were cultured through continuous culture using Dulbecco's Modified Eagle's Medium (DMEM, Sigma Chemical Co., St. Louis, MO) supplemented with 10% fetal bovine serum (Invitrogen), penicillin (100 μg/mL), and streptomycin (100 μg/mL). Cells were cultured in 75 cm^2 filter-capped tissue culture flask, made up with polystyrene, in CO_2 incubator with 5% CO_2 and 95% air at 37 °C. From the logarithmically grown culture, the cell density was adjusted to 10^5 per/well with fresh media. The cells were then used to inoculate in a glass bottom dish, with 1.0 mL (10^4 cells) of cell suspension. After cell adhesion, culture medium was removed. The cell layer was rinsed twice with phosphate buffered saline (PBS) (pH 7.0), and then treated according to the experimental need.

Cell imaging study: For microscopic studies, 10^4 HuH-7 cells in 1 mL of medium were seeded on three sterile 35 mm glass bottom culture dish (ibidi GmbH, Germany), and incubated at 37 °C in a CO_2 incubator for 10 h. Then cells were washed with 500 mL of fresh DMEM medium followed by incubation with the **H_2BIo** (1 μM), dissolved in 1000 μL DMEM, at 37 °C for 1 h in a CO_2 incubator. Cells were washed thrice with phosphate buffered saline (PBS) (pH 7.0)

to remove excess **H_2BIo** observed under an Olympus IX73 fluorescence microscope. Images obtained were analyzed by FITC filter with excitation at 360 nm, and emission spectra were integrated over the range 520 nm. The cells were further incubated with Cu^{2+} (2.5 μM) for 20 min and excess Cu^{2+} was washed thrice with PBS (pH 7.0) followed by analyses under fluorescence microscope. We have performed similar experiments with **H_3BIdm** and **H_2BIp** also. For all the images, the fluorescence microscope settings, such as transmission density and scan speed were held constant to compare the relative intensity of the intracellular fluorescence.

Synthesis

Synthesis of 2-(1H-benzoimidazol-2-yl)-4-methyl-phenol (HBI): To a 15 mL methanolic solution of 2-hydroxy-5-methylbenzaldehyde (5 mmol, 0.680 g), $NaHSO_3$ (15 mmol, 2 g) was added and stirred for 3 h. A 15 mL DMF solution of *o*-phenylenediamine (5 mmol, 0.504 g) was slowly added to the previous solution and the mixed solution was further stirred at 80 °C for another 2 h. After cooling at room temperature, the reaction mixture was added to 500 mL distilled water and off-white solid was precipitated out. The product was filtered and washed many times with water. After complete drying the product was recrystallised in methanol and white needle shaped crystals were obtained after one day. Yield: 84%. C, 74.98; H, 5.39; N, 12.49%. Found: C, 74.91; H, 5.34; N, 12.56. ^{1}H NMR (DMSO-d_6, 300 MHz): δ (ppm): 12.95(2H, s), 7.89(1H, s), 7.66(2H, brs), 7.29–7.26(2H, m), 7.20–7.16(1H, m), 6.96–6.93(1H, d) and 2.33(3H, s). ^{13}C NMR (DMSO-d_6, 75 MHz): δ (ppm): 156.38, 152.26, 132.87, 128.13, 126.64, 123.34, 118.55, 117.45, 112.69 and 20.58. ESI-MS: *m/z*, 225.0431 amu (calc.: 225.1028) [(HBI + H)$^+$]. FT-IR:$\nu_{(O-H)}$ and $\nu_{(N-H)} = 3292$ cm^{-1}.

Synthesis of 3-(1H-benzoimidazol-2-yl)-2-hydroxy-5-methyl-benzaldehyde (HBIA): 3-(1H-benzoimidazol-2-yl)-2-hydroxy-5-methyl-benzaldehyde (HBIA) was synthesized according to a reported method.[46] Hexamethylenetetramine (2.26 g, 16.1 mmol) was added to a stirred solution of HBI (604 mg, 2.69 mmol) dissolved in 15 mL of CF_3CO_2H and refluxed for 27 h. After cooling to room temperature, water was added to quench the reaction. Yellow solid was collected by filtration and washed with water. Diffraction quality yellow needle shaped crystals were obtained from saturated solution of the HBIA in DMSO during the time period of 5 days. Yield: 87%. C, 71.42; H, 4.79; N, 11.10%. Found: C, 71.46; H, 4.72; N, 11.07. ^{1}H NMR (DMSO-d_6, 300 MHz): δ (ppm): 10.43(1H, s), 8.14(1H, s), 7.70–7.67(2H, q), 7.58 (1H, s), 7.34–7.31(2H, q) and 2.34(3H, s). ^{13}C NMR (DMSO-d_6, 75 MHz): δ (ppm): 189.79, 159.54, 150.87, 136.78, 133.33, 130.35, 128.38, 123.91, 123.84, 115.24, 114.22 and 20.39. ESI-MS: *m/z*, 254.0280 amu (calc.: 253.0977) [(HBIA + H)$^+$]. FT-IR: $\nu_{(C=O)} = 1663$ cm^{-1}, $\nu_{(O-H)}$ and $\nu_{(N-H)} = 3337$ cm^{-1}.

Synthesis of 2-{[3-(1H-benzoimidazol-2-yl)-2-hydroxy-5-methyl-benzylidene]-amino}-benzoic acid (H_2BIo): To a 10 mL methanolic solution of 3-(1H-benzoimidazol-2-yl)-2-hydroxy-5-methyl-benzaldehyde (HBIA) (1 mmol, 0.252 g), anthranilic acid (1 mmol, 0.137 g) was added and refluxed for 6 h. The reaction mixture was cooled at room temperature and then placed it at 4 °C for overnight. A red solid product was obtained after filtration and dried under vacuum. Yield: 79%. C, 71.15; H, 4.61; N, 11.31%. Found: C, 71.34; H, 4.67; N, 11.17. ^{1}H NMR (DMSO-d_6, 300 MHz): δ (ppm): 10.45(1H, s), 8.14(1H, s), 7.71(1H, s), 7.68–7.65(2H, m), 7.55(1H, s), 7.32–7.29(2H, m), 7.24–7.19(1H, t), 6.76–6.73(1H, d), 6.53–6.48(1H, t) and 2.33 (3H, s). ^{13}C NMR (DMSO-d_6, 75 MHz): δ (ppm): 189.47, 170.04, 159.68, 151.95, 151.17, 134.16, 133.13, 131.62, 129.95, 128.26, 123.96, 123.68, 116.79, 115.03, 114.35, 110.08 and 20.40. ESI-MS: *m/z*, 372.1515 amu (calc.: 372.1348) [(**H_2BIo** + H)$^+$]. FT-IR: $\nu_{(C=O)} = 1675$ cm^{-1}, $\nu_{(C=N)} = 1620$ cm^{-1}, $\nu_{(C-O)} = 1240$ cm^{-1}, $\nu_{(O-H)}$ and $\nu_{(N-H)} = 3472$ cm^{-1}.

Synthesis of 5-{[3-(1H-benzoimidazol-2-yl)-2-hydroxy-5-methyl-benzylidene]-amino}-isophthalic acid (H_3BIdm): 5-{[3-(1H-benzoimidazol-2-yl)-2-hydroxy-5-methyl-benzylidene]-amino}-isophthalic acid (**H_3BIdm**) was prepared according to similar procedure of **H_2BIo** taking 5-aminoisophthalic acid (1 mmol, 0.181 g) in place of anthranilic acid. The product was recrystallised in methanol and orange block shaped single crystals were obtained after two days. Yield: 77%. C, 66.41; H, 4.18; N, 10.08%. Found: C, 66.50; H, 4.12; N, 10.12. ^{1}H NMR (DMSO-d_6, 300 MHz): δ (ppm): 10.44(1H, s), 8.12–8.10(2H, d), 8.05 (1H, s), 7.68–7.63(3H, m), 7.38(1H, s), 7.31–7.27(2H, m), and 2.32 (3H, s). ^{13}C NMR (DMSO-d_6, 75 MHz): δ (ppm): 189.47, 167.69, 166.72, 159.68, 158.24, 151.19, 149.65, 133.04, 132.12, 129.91, 128.27, 126.12, 123.95, 123.67, 118.67, 114.35 and 20.40. ESI-MS: *m/z*, 416.1856 amu (calc.: 416.4061) [(**H_3BIdm** + H)$^+$]. FT-IR: $\nu_{(C=O)} = 1726$ and 1676 cm^{-1}, $\nu_{(C-O)} = 1190$ cm^{-1},$\nu_{(C=N)} = 1625$ cm^{-1}, $\nu_{(O-H)}$ and $\nu_{(N-H)} = 3407$ cm^{-1}.

Synthesis of 4-{[3-(1H-benzoimidazol-2-yl)-2-hydroxy-5-methyl-benzylidene]-amino}-benzoic Acid (H_2BIp): 4-{[3-(1H-benzoimidazol-2-yl)-2-hydroxy-5-methyl-benzylidene]-amino}-benzoic acid (**H_2BIp**) was prepared according to similar procedure as **H_2BIo** taking 4-aminobenzoic acid (1 mmol, 0.137 g) in place of anthranilic acid. Yield: 75%. C, 71.15; H, 4.61; N, 11.31%. Found: C, 71.31; H, 4.69; N, 11.21. ^{1}H NMR (DMSO-d_6, 300 MHz): δ (ppm): 10.45(1H, s), 8.13(1H, s), 7.69–7.62(4H, m), 7.55(1H, s), 7.32–7.28(2H, m), 6.58–6.55(2H, d) and 2.33 (3H, s). ^{13}C NMR (DMSO-d_6, 75 MHz): δ (ppm): 189.45, 167.99, 167.41, 157.83, 133.09, 132.07, 131.69, 131.25, 129.89, 128.26, 123.96, 123.67, 121.57, 117.37, 114.36, 113.05 and 20.41. ESI-MS: *m/z*, 372.1476 amu (calc.: 372.1348) [(**H_2BIp** + H)$^+$]. FT-IR: $\nu_{(C=O)} = 1675$ cm^{-1}, $\nu_{(C=N)} = 1600$ cm^{-1}, $\nu_{(C-O)} = 1176$ cm^{-1}, $\nu_{(O-H)}$ and $\nu_{(N-H)} = 3369$ cm^{-1}.

Synthesis of [(BIo)$_2$Cu$_2$] complex (1): To a 5 mL methanolic solution of **H_2BIo** (0.1 mmol, 37.1 mg), $CuCl_2 \cdot 2H_2O$ (0.1 mmol, 17 mg) was added followed by addition of triethylamine (0.1 mmol, 13.8 μL) and the reaction mixture was stirred for 3 h. Green solid of **1** was obtained after filtration and the solid was washed with cold methanol. Yield: 62%. ESI-MS: *m/z*, 433.0505 (calc.: 433.0588) [(HBIo)Cu]$^+$; 865.0859 (calc.: 865.1097) [(BIo)$_2$Cu$_{2+}$H]$^+$. FT-IR: $\nu_{(C=O)}$ and$\nu_{(C=N)} = 1550$ cm^{-1}, $\nu_{(C-O)} = 1080$ cm^{-1}and $\nu_{(N-H)} = 3414$ cm^{-1}.

Synthesis of [(HBIdm)$_2$Cu$_2$] complex (2): [(HBIdm)$_2$Cu$_2$] (**2**) was synthesized following same procedure by using **H_3BIdm** in place of **H_2BIo**. Yield: 66%. ESI-MS: *m/z*, 477.0455 (calc.: 477.0486) [(H$_2$BIdm)Cu]$^+$; 955.0247 (calc.: 955.1050) [(HBIdm)$_2$Cu$_{2+}$H]$^+$. FT-IR: $\nu_{(C=O)} = 1708$ and 1631 cm^{-1}, $\nu_{(C=N)} = 1560$ cm^{-1}, $\nu_{(C-O)} = 1086$ cm^{-1},$\nu_{(O-H)}$ and $\nu_{(N-H)} = 3430$ cm^{-1}.

Synthesis of $[(Blp)_2Cu_2]$ complex (3): $[(Blp)_2Cu_2]$ (**3**) was obtained similarly to $[(Blo)_2Cu_2]$ (**1**), by using **H_2Blp** in place of **H_2Blo**. Yield: 66%. ESI-MS: *m/z*, 433.0548 (calc.: 433.0588) $[(HBlp)Cu]^+$; 865.0920 (calc.: 865.1097) $[(Blp)_2Cu_{2+}H]^+$. FT-IR: $\nu_{(C=O)} = 1632\ cm^{-1}$, $\nu_{(C=N)} = 1562\ cm^{-1}$, $\nu_{(C-O)} = 1112\ cm^{-1}$ and $\nu_{(N-H)} = 3407\ cm^{-1}$.

Sample preparation for spectral studies: The stock solution of **H_2Blo** (10^{-3} M), **H_3Bldm** (10^{-3} M) and **H_2Blp** (10^{-3} M) were prepared in different organic solvents. The stock solutions of various metal ions (10^{-3} M) were prepared by using their perchlorate or chloride salts in triple distilled water. For emission and absorption experiments, final concentrations of probes were maintained as 0.1 μM and 10 μM respectively. The required amount of metal ion stock solutions were added using a micropipette to the probe solution in the whole spectral analysis. Spectral data were recorded at 1 minute interval after the addition of the metal ions.

Acknowledgements

RB and MMI are thankful to the University Grants Commission, New Delhi, India (Sanction No. F1-17.1/2017-18/RGNF-2017-18-SC-WES-37660/(SA-III/Website) and UGC Ref No.712/CSIR-UGC NET DEC.2017 respectively) for the financial support. SS acknowledges Shailabala Biswas Research Foundation, University of Calcutta, Kolkata, India. DST-FIST and DST-PURSE are acknowledged for providing single crystal XRD and ESI-MS facility at the Department of Chemistry, University of Calcutta. SG is grateful to CAS-V(UGC), of the Department of Chemistry, University of Calcutta, for financial assistance. We are grateful to Prof. Anindya Dutta (Department of Chemistry, IIT Bombay, India) and his group for their valuable contribution in Time-correlated single photon counting (TCSPC) and solid fluorescence measurements. We are also thankful to Prof. Debabrata Mandal (Department of Chemistry, University of Calcutta, India) for allowing us to access the spectrofluorimeter for emission experiment.

Conflict of Interest

The authors declare no conflict of interest.

Data Availability Statement

The data that support the findings of this study are available from the corresponding author upon reasonable request.

Keywords: Benzimidazole · Aminobenzoic acids · ESIPT · C=N isomerization · Cu^{2+} sensor

[1] J. E. Kwon, S. Y. Park, *Adv. Mater.* **2011**, *23*, 3615–3642.
[2] J. Zhao, S. Ji, Y. Chen, H. Guo, P. Yang, *Phys. Chem. Chem. Phys.* **2012**, *14*, 8803–8817.
[3] A. Weller, *Z. Elektrochem.* **1956**, *60*, 1144–1147.
[4] A. C. Sedgwick, L. Wu, H. Han, S. D. Bull, X. He, T. D. James, J. L. Sessler, B. Z. Tang, H. Tian, J. Yoon, *Chem. Soc. Rev.* **2018**, *47*, 8842–8880.
[5] Y. Zheng, H. Zhang, D. Tian, D. Duan, F. Dai, B. Zhou, *Spectrochim. Acta A* **2020**, *238*, 118429.
[6] Q. Zheng, F. Ding, X. Hu, J. Feng, J. Shen, X. He, *Bioorg. Chem.* **2021**, *109*, 104746.
[7] D. Jiang, M. Zheng, X. Yan, B. Huang, H. Huang, T. Gong, K. Liu, J. Liu, *RSC Adv.* **2022**, *12*, 31186–31191.
[8] H. Ren, F. Huo, W. Wen, C. Yin, *Dyes Pigm.* **2022**, *199*, 110111.
[9] H. Ren, F. Huo, X. Wu, X. Liu, C. Yin, *Chem. Commun.* **2021**, *57*, 655–658.
[10] C. Bao, S. Shao, H. Zhou, Yifeng Han, *New J. Chem.* **2021**, *45*, 10735–10740.
[11] F. Fan, C. Xu, X. Liu, M. Zhu, Y. Wang, *Spectrochim. Acta A* **2022**, *280*, 121499.
[12] H. Zhuang, W. Shi, G. Zhao, Y. Yang, Y. Li, *Spectrochim. Acta A* **2022**, *282*, 121650.
[13] X. Tang, X. Zhu, H. Xu, H. Sun, X. Han, Q. Li, B. Zhou, Z. Ni, *Spectrochim. Acta A* **2022**, *281*, 121567.
[14] R. Wang, D. Liu, K. Xu, J. Li, *J. Photochem. Photobiol. A* **2009**, *205*, 61–69.
[15] L. Zhang, L. Qi, X. Chen, F. Liu, L. Liu, W. Ding, D. Li, G. Yuan, J. Tong, F. Chen, H. Huang, Y. Wang, *J. Chem. Crystallogr.* **2019**, *49*, 260–266.
[16] Y. Jiao, X. Liu, L. Zhou, H. He, P. Zhou, C. Duan, *Sens. Actuators B* **2017**, *247*, 950–956.
[17] M. Hranjec, G. Pavlovic, M. Marjanovic, M. Kralj, G. Karminski-Zamola, *Eur. J. Med. Chem.* **2010**, *45*, 2405–2417.
[18] K. Sakai, H. Kawamura, N. Kobayashi, T. Ishikawa, C. Ikeda, T. Kikuchi, T. Akutagawa, *CrystEngComm* **2014**, *16*, 3180–3185.
[19] K. Sakai, S. Tsuchiya, T. Kikuchi, T. Akutagawa, *J. Mater. Chem. C* **2016**, *4*, 2011–2016.
[20] F. S. Rodembusch, F. P. Leusin, L. F. Campo, V. Stefani, *J. Lumin.* **2007**, *126*, 728–734.
[21] H. A. Benesi, J. H. Hildebrand, *J. Am. Chem. Soc.* **1949**, *71*, 2703–2707.
[22] J. Hatai, S. Pal, G. P. Jose, T. Sengupta, S. Bandyopadhyay, *RSC Adv.* **2012**, *2*, 7033–7036.
[23] M. R. Hasan, M. A. Hossain, M. A. Salam, M. N. Uddin, *J. Taibah Univ. Sci.* **2016**, *10*, 766–773.
[24] T. Suksrichavalit, S. Prachayasittikul, T. Piacham, C. Isarankura-Na-Ayudhya, C. Nantasenamat, V. Prachayasittikul, *Molecules* **2008**, *13*, 3040–3056.
[25] J. Ratha, K. A. Majumdar, S. K. Mandal, R. Bera, C. Sarkar, B. Saha, C. Mandal, K. D. Saha, R. Bhadra, *Mol. Cell. Biochem.* **2006**, *290*, 113–123.
[26] A. M. Brouwer, *Pure Appl. Chem.* **2011**, *83*, 2213–2228.
[27] F. Neese, *Wiley Interdiscip. Rev. Comput. Mol. Sci.* **2012**, *2*, 73–78.
[28] F. Neese, *Wiley Interdiscip. Rev.: Comput. Mol. Sci.* **2018**, *8*, e1327.
[29] M. D. Hanwell, D. E. Curtis, D. C. Lonie, T. Vandermeersch, E. Zurek, G. R. Hutchison, *J. Cheminform.* **2012**, *4*, 17.
[30] R. G. Parr, W. Yang in *Density Functional Theory of Atoms and Molecules*, Oxford University Press, Oxford, **1989**.
[31] D. R. Salahub, M. C. Zerner in *the Challenge of d and f Electrons*, American Chemical Society: Washington, DC, **1989**.
[32] W. Kohn, L. Sham, *Phys. Rev.* **1965**, *140*, A1133–A1138.
[33] P. Hohenberg, W. Kohn, *Phys. Rev.* **1964**, *136*, B864–B871.
[34] F. Weigend, R. Ahlrichs, *Phys. Chem. Chem. Phys.* **2005**, *7*, 3297–3305.
[35] F. Weigend, F. Furche, R. Ahlrichs, *J. Chem. Phys.* **2003**, *119*, 12753–12762.
[36] K. Eichkorn, F. Weigend, O. Treutler, R. Ahlrichs, *Theor. Chem. Acc.* **1997**, *97*, 119–124.
[37] A. Schäefer, C. Huber, R. Ahlrichs, *J. Chem. Phys.* **1994**, *100*, 5829–5835.
[38] A. Schäefer, H. Horn, R. Ahlrichs, *J. Chem. Phys.* **1992**, *97*, 2571–2577.
[39] F. A. Weigend, *Phys. Chem. Chem. Phys.* **2002**, *4*, 4285–4291.
[40] F. Weigend, M. Häser, H. Patzelt, R. Ahlrichs, *Chem. Phys. Lett.* **1998**, *294*, 143–152.
[41] J. L. Whitten, *J. Chem. Phys.* **1973**, *58*, 4496–4501.
[42] H. B. Schlegel, J. J. McDouall in *Computational Advances in Organic Chemistry*, Kluwer Academic, The Netherlands, **1991**.
[43] V. Barone, M. Cossi, *J. Phys. Chem. A* **1998**, *102*, 1995–2001.
[44] G. M. Sheldrick, *SADABS 2.05*,University of Göttingen, Göttingen, Germany.
[45] G. M. Sheldrick, *Acta Cryst.* **2015**, *C71*, 3–8.
[46] T. Honda, Y. Ishida, T. Arai, *Bull. Chem. Soc. Jpn.* **2016**, *89*, 1321–1327.

Manuscript received: November 2, 2022
Accepted manuscript online: February 7, 2023
Version of record online: March 16, 2023